Journal of
Mechanics of
Materials and Structures

NONLINEAR FLUTTER INSTABILITY OF THIN DAMPED PLATES: A SOLUTION BY THE ANALOG EQUATION METHOD

John T. Katsikadelis and Nick G. Babouskos

Volume 4, Nº 7-8 September 2009

mathematical sciences publishers

JOURNAL OF MECHANICS OF MATERIALS AND STRUCTURES
Vol. 4, No. 7-8, 2009

NONLINEAR FLUTTER INSTABILITY OF THIN DAMPED PLATES: A SOLUTION BY THE ANALOG EQUATION METHOD

JOHN T. KATSIKADELIS AND NICK G. BABOUSKOS

We investigate the nonlinear flutter instability of thin elastic plates of arbitrary geometry subjected to a combined action of conservative and nonconservative loads in the presence of both internal and external damping and for any type of boundary conditions. The response of the plate is described in terms of the displacement field by three coupled nonlinear partial differential equations (PDEs) derived from Hamilton's principle. Solution of these PDEs is achieved by the analog equation method (AEM), which uncouples the original equations into linear, quasistatic PDEs. Specifically, these are a biharmonic equation for the transverse deflection of the plate, that is, the bending action, plus two linear Poisson's equations for the accompanying in-plane deformation, that is, the membrane action, under time-dependent fictitious loads. The fictitious loads themselves are established using the domain boundary element method (D/BEM). The resulting system for the semidiscretized nonlinear equations of motion is first transformed into a reduced problem using the aeroelastic modes as Ritz vectors and then solved by a new AEM employing a time-integration algorithm. A series of numerical examples is subsequently presented so as to demonstrate the efficiency of the proposed methodology and to validate the accuracy of the results. In sum, the AEM developed herein provides an efficient computational tool for realistic analysis of the admittedly complex phenomenon of flutter instability of thin plates, leading to better understanding of the underlying physical problem.

1. Introduction

The stability of thin plates subjected to conservative as well as nonconservative loads is of great importance in many fields of engineering such as aircrafts, space structures, mechanical, and civil engineering applications. The combined action of conservative and nonconservative loads, such as follower forces and aerodynamic pressure, initiate flutter instability in the plate that manifests itself in the form of vibrations with ever-increasing amplitude as time goes. Basically, flutter is a self-excited oscillation which occurs in systems which are not subjected to periodic forces. Linear plate theory indicates that there is a critical value of load above which the plate becomes unstable and the displacements grow exponentially with time. However, as the deflection of the plate increases, the membrane stresses pick up considerably in magnitude and limit the motion to a bounded value with increasing amplitude as the load level increases. Hence, we have to consider the nonlinear plate problem in order to have a better insight to this type of instability. In presence of damping, be it internal or external, the plate becomes unstable at the critical value of the nonconservative forces and reaches a periodic motion, known as limit cycle oscillation, which is independent of the initial displacements.

Keywords: nonlinear flutter, plates, aeroelasticity, instability, follower forces, boundary elements, analog equation method, aerodynamic loads.

The linear flutter of plates has been examined by many authors who used analytic and approximate techniques. Leipholz and Pfendt [1983] studied the flutter instability of rectangular plates with various types of boundary conditions under uniformly distributed follower forces. Adali [1982] investigated the flutter and divergence instability of a rectangular plate on an elastic foundation where he found that the type of instability depends on the combination of the conservative and nonconservative loads, the Poisson's ratio, the foundation moduli and the plate aspect ratio. Higuchi and Dowell [1992] were among the first researchers to investigate the destabilizing effect of structural damping on flutter instability of plates. Zuo and Schreyer [1996] studied the flutter and divergence instability of beams and thin rectangular plates under the combined action of conservative and nonconservative loads. Kim and Kim [2000] used the finite element method (FEM) to analyze Kirchhoff and Mindlin type of plates under follower forces.

The linear and nonlinear flutter of plates subjected to aerodynamic pressure has been also the subject of many investigators due to the importance of this type of instability in flight vehicles traveling at supersonic Mach numbers. For instance, Dowell [1966] studied the nonlinear oscillations of a plate that is subjected to in-plane loads and aerodynamic pressure according to quasisteady supersonic flow theory. Next, Mei [1977] also studied this problem using the FEM, while Shiau and Lu [1990] investigated the nonlinear flutter of composite laminated plates. The limit cycle oscillations of a thin isotropic rectangular plate exposed to supersonic air flow has been also investigated by many authors [Weiliang and Dowell 1991; Guo and Mei 2003; Chen et al. 2008]. Due to the complexity of the governing equations, only approximate and numerical techniques such as the Rayleigh–Ritz method and the FEM have been used, which however treat plates with relatively simple geometry (rectangular, triangular) under simple load distributions and boundary (support) conditions. Finally, the linear flutter and divergence instability of a plate of arbitrary geometry with any type of boundary conditions has been investigated recently by Babouskos and Katsikadelis [2009].

In this paper the problem of nonlinear flutter instability of plates of any type of geometry subjected to arbitrary boundary conditions under interior and edge conservative and nonconservative loads of follower type is solved in presence of internal (structural) and external (viscous) damping. The equations of the plate are derived by using Hamilton's principle and considering nonlinear kinematic relations resulting from the von Kármán assumption. The resulting initial-boundary value problem consisting of three coupled nonlinear hyperbolic PDEs in terms of displacements with nonlinear boundary conditions is solved using the AEM developed in [Katsikadelis 1994; 2002], which converts the original equations into three linear uncoupled quasistatic PDEs, namely a linear plate (biharmonic) equation for the transverse deflection and two linear (Poisson) membrane equations for the membrane (in-plane) deformation. The new problem employs time-dependent fictitious loads that are established using the D/BEM, under the original boundary conditions. This procedure results in an initial value problem of nonlinear equations of motion for the discretized fictitious sources, whose solution is achieved by transformation to a reduced problem using Ritz vectors. The aeroelastic modes, namely the eigenmodes of the linear flutter plate problem near the critical point and in absence of damping, are selected as Ritz vectors [Guo and Mei 2003]. The reduced initial value problem is solved using a new AEM time step integration algorithm [Katsikadelis 2009]. Finally, the response of the plate is established from the integral representation of the substitute problems. In terms of examples, the vibration of plates under a given initial disturbance plus the action of the conservative and nonconservative forces and the ensuing postcritical behavior

is examined. These numerical examples demonstrate the efficiency and validate the accuracy of the methodology. Useful conclusions are drawn, which validate also the findings of earlier investigators. In sum, the present method provides a computational tool for a realistic analysis and better understanding of the complex phenomenon of nonlinear flutter instability of plates in the presence of damping. Although the membrane inertia forces were ignored here, the solution procedure permits their inclusion and their influence will be the subject of a forthcoming paper.

2. Governing equations

2.1. ***The nonlinear plate problem.*** Consider a thin elastic plate of uniform thickness h occupying the two dimensional multiply connected domain Ω of the xy plane with boundary $\Gamma = \bigcup_{i=0}^{K} \Gamma_i$ (Figure 1). The curves Γ_i $(i = 0, 1, 2, \ldots, K)$ may be piecewise smooth. The boundary may be simply supported, clamped, free, or elastically supported with transverse stiffness $k_T(x)$ and rotational stiffness $k_R(x)\boldsymbol{x}$: $(x, y) \in \Gamma$, respectively. The plate is subjected to in-plane conservative n_x, n_y, and/or nonconservative loads p_x, p_y (body forces) as well as to aerodynamic pressure Δp due to air flow. Moreover, along the movable edges conservative N_n^*, N_t^* and nonconservative P_n^*, P_t^* forces may be applied. The von Kármán assumption for the kinematic relation is adopted:

$$\varepsilon_x = u_{,x} + \tfrac{1}{2} w_{,x}^2, \quad \varepsilon_y = v_{,y} + \tfrac{1}{2} w_{,y}^2, \quad \gamma_{xy} = u_{,y} + v_{,x} + w_{,x} w_{,y}, \tag{2-1}$$

where $u = u(x, y, t)$ and $v = v(x, y, t)$ are the membrane displacements and $w = w(x, y, t)$ the transverse displacement.

Quasisteady supersonic first-order piston theory is employed for the aerodynamic pressure; it gives a good approximation for high supersonic Mach numbers [Dowell 1966; Mei 1977; Guo and Mei 2003].

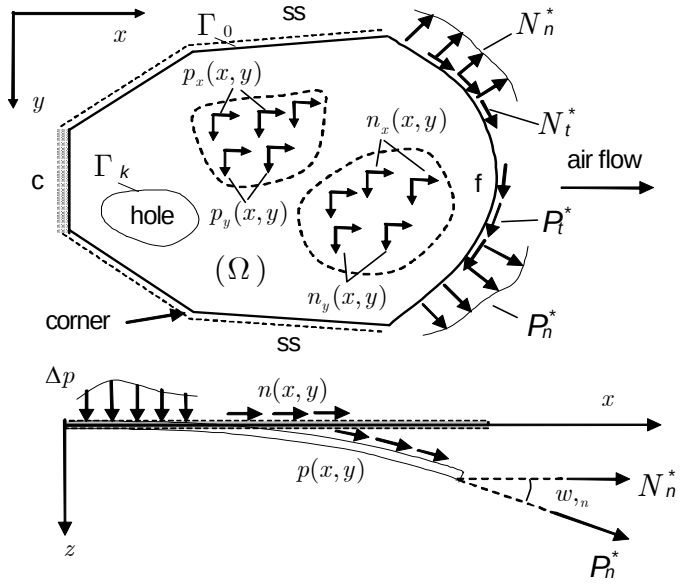

Figure 1. Plate geometry and supports (c = clamped, ss = simply supported, f = free).

In this case the pressure is

$$\Delta p = -(q_x w_{,x} + q_y w_{,y} + c\dot{w}), \tag{2-2}$$

where q_x, q_y, and c are parameters depending on the density, the velocity and the direction of the air flow and are given in [Guo and Mei 2003]. Neglecting in-plane inertia and damping forces, the governing equations and the boundary conditions of the problem are obtained from Hamilton's principle, which in this case reads

$$\int_{t_1}^{t_2} (\delta T - \delta U + \delta V + \delta W_{nc})\, dt = 0, \tag{2-3}$$

where T, U are the kinetic and elastic energy and V the potential of the external forces:

$$T = \frac{1}{2}\int_\Omega \rho h \dot{w}^2 \, d\Omega, \tag{2-4}$$

$$U = \frac{D}{2}\int_\Omega \left(w_{,xx}^2 + w_{,yy}^2 + 2\nu w_{,xx} w_{,yy} + 2(1-\nu) w_{,xy}^2\right) d\Omega + \frac{1}{2}\int_\Gamma (k_T w^2 + k_R w_{,n}^2)\, ds \tag{2-5}$$

$$+\frac{C}{2}\int_\Omega \left(\left(u_{,x}+\tfrac{1}{2}w_{,x}^2\right)^2 + \left(v_{,y}+\tfrac{1}{2}w_{,y}^2\right)^2 + 2\nu\left(u_{,x}+\tfrac{1}{2}w_{,x}^2\right)\left(v_{,y}+\tfrac{1}{2}w_{,y}^2\right) + \frac{1-\nu}{2}\left(u_{,y}+v_{,x}+w_{,x}w_{,y}\right)^2\right) d\Omega,$$

$$V = -\int_\Omega \left[(n_x + p_x)u + (n_y + p_y)v\right] d\Omega - \int_\Gamma \left((N_n^* + P_n^*)u_n + (N_t^* + P_t^*)u_t\right) ds. \tag{2-6}$$

Here δW_{nc} is the virtual work of the nonconservative loads and the external and internal damping forces, written as

$$\delta W_{nc} = \int_\Omega \left((p_x - q_x)w_{,x} + (p_y - q_y)w_{,y}\right)\delta w \, d\Omega + \int_\Gamma (P_n^* w_{,n} + P_t^* w_{,t})\,\delta w \, ds - \int_\Omega c\dot{w}\,\delta w \, d\Omega$$
$$- \int_\Omega \eta D\left((\dot{w}_{,xx} + \nu \dot{w}_{,yy})\delta w_{,xx} + (\dot{w}_{,yy} + \nu \dot{w}_{,xx})\delta w_{,yy} + 2(1-\nu)\dot{w}_{,xy}\,\delta w_{,xy}\right) d\Omega, \tag{2-7}$$

where $c = c(x, y)$ and $\eta = \eta(x, y)$ are the external damping and internal damping coefficients, $\rho = \rho(x, y)$ is the material density of the plate, $D = Eh^3/12(1-\nu^2)$ is the flexural rigidity with E, ν being the Young's modulus and Poisson's ratio, respectively, and $C = Eh/(1-\nu^2)$ is the membrane stiffness of the plate.

Introducing (2-4)–(2-7) into (2-3), using the calculus of variations, performing the necessary integrations by parts, and ignoring the time-dependent terms in the boundary conditions, we obtain the following initial and boundary value problems:

(i) For the transverse deflection,

$$D\nabla^4 w - (N_x w_{,xx} + 2N_{xy} w_{,xy} + N_y w_{,yy}) + (q_x + n_x)w_{,x} + (q_y + n_y)w_{,y} + \rho h\ddot{w} + c\dot{w} + \eta D\nabla^4 \dot{w} = 0 \quad \text{in } \Omega, \tag{2-8}$$

$$w(\boldsymbol{x}, 0) = g_1(\boldsymbol{x}), \quad \dot{w}(\boldsymbol{x}, 0) = g_2(\boldsymbol{x}) \quad \text{in } \Omega, \tag{2-9}$$

$$V w + N_n^* w_{,n} + N_t^* w_{,t} + k_T w = 0 \ \text{ or } \ w = 0 \qquad \text{on } \Gamma, \tag{2-10a}$$

$$M w - k_R w_{,n} = 0 \ \text{ or } \ w_{,n} = 0 \qquad \text{on } \Gamma, \tag{2-10b}$$

$$k_T^{(k)} w^{(k)} - [\![T w]\!]_k = 0 \ \text{ or } \ w^{(k)} = 0 \qquad \text{at corner point } k, \tag{2-10c}$$

(ii) For the in-plane deformation,

$$\left.\begin{aligned} \nabla^2 u + \frac{1+\nu}{1-\nu}(u_{,x} + v_{,y})_{,x} + w_{,x}\left(\frac{2}{1-\nu} w_{,xx} + w_{,yy}\right) + \frac{1+\nu}{1-\nu} w_{,xy} w_{,y} + \frac{n_x + p_x}{Gh} = 0 \\ \nabla^2 v + \frac{1+\nu}{1-\nu}(u_{,x} + v_{,y})_{,y} + w_{,y}\left(\frac{2}{1-\nu} w_{,yy} + w_{,xx}\right) + \frac{1+\nu}{1-\nu} w_{,xy} w_{,x} + \frac{n_y + p_y}{Gh} = 0 \end{aligned}\right\} \text{ in } \Omega, \tag{2-11}$$

$$\left.\begin{aligned} N_n = N_n^* + P_n^* \ \text{ or } \ u_n = u_n^* \\ N_t = N_t^* + P_t^* \ \text{ or } \ u_t = u_t^* \end{aligned}\right\} \text{ on } \Gamma, \tag{2-12}$$

where $G = E/2(1+\nu)$ is the shear modulus, $V w$ is the equivalent shear force, $M w$ is the normal bending moment, $T w$ is the twisting moment along the boundary, while $[\![T w]\!]_k$ is its discontinuity jump at corner k. The operators producing these quantities are given as

$$V = -D\left(\frac{\partial}{\partial n}\nabla^2 + (1-\nu)\frac{\partial}{\partial s}\left(\frac{\partial^2}{\partial s\,\partial n} - \kappa\frac{\partial}{\partial s}\right)\right), \tag{2-13a}$$

$$M = -D\left(\nabla^2 - (1-\nu)\left(\frac{\partial^2}{\partial s^2} + \kappa\frac{\partial}{\partial n}\right)\right), \tag{2-13b}$$

$$T = D(1-\nu)\left(\frac{\partial^2}{\partial s\,\partial n} - \kappa\frac{\partial}{\partial s}\right), \tag{2-13c}$$

where $\kappa = \kappa(s)$ is the curvature of the boundary and n, s are the intrinsic boundary coordinates. Finally, the quantities N_x, N_y, N_{xy} represent the in-plane membrane forces given as

$$N_x = C(\varepsilon_x + \nu\varepsilon_y), \quad N_y = C(\varepsilon_y + \nu\varepsilon_x), \quad N_{xy} = C\frac{1-\nu}{2}\gamma_{xy}. \tag{2-14}$$

2.2. ***The linear plate problem.*** The plate problem is linearized if the stretching of the middle surface due to bending is neglected, that is if it is set $w_{,x}^4 = w_{,y}^4 = w_{,x}^2 w_{,y}^2 \simeq 0$ in (2-5). This implies that although the in-plane forces contribute to bending they are not influenced by it. Thus the nonlinear terms in (2-11) vanish. The boundary conditions are the same for both problems. Apparently, in this case the two problems are uncoupled. Therefore, the in-plane forces N_x, N_y, N_{xy} are obtained from the linearized equations (2-11), which are solved independently. The solution of the linear problem is required because the eigenmodes of the resulting eigenvalue problem are employed for the solution of the nonlinear equations of motion (Section 3.4).

3. The AEM solution

3.1. ***The plate problem.*** The initial boundary value problem (2-8)–(2-10) for the dynamic response of the plate is solved using the AEM [Katsikadelis 1994]. The analog equation for the problem at hand is

$$\nabla^4 w = b(\boldsymbol{x}, t), \quad \boldsymbol{x} = \{x, y\} \in \Omega, \tag{3-1}$$

where $b(\boldsymbol{x}, t)$ represents the time-dependent fictitious load. Equation (3-1) is a quasistatic equation, that is, the time appears as a parameter, and it can be solved with the boundary conditions (2-10) at any instant t using the BEM. Thus, the solution at a point $\boldsymbol{x} \in \Omega$ is obtained in integral form as

$$w(\boldsymbol{x}, t) = \int_\Omega w^* b \, d\Omega + \int_\Gamma \left(w^* V w + w_{,n} M w^* - w^*_{,n} M w - w V w^* \right) ds - \sum_k \left(w^* [\![T w]\!] - w [\![T w^*]\!] \right)_k, \quad (3\text{-}2)$$

which for $\boldsymbol{x} \in \Gamma$ yields the following two boundary integral equations for points where the boundary is smooth:

$$\tfrac{1}{2} w(\boldsymbol{x}, t) = \int_\Omega w^* b \, d\Omega + \int_\Gamma \left(w^* V w + w_{,n} M w^* - w^*_{,n} M w - w V w^* \right) ds - \sum_k \left(w^* [\![T w]\!] - w [\![T w^*]\!] \right)_k, \quad (3\text{-}3)$$

$$\tfrac{1}{2} w_{,\boldsymbol{\nu}}(\boldsymbol{x}, t) = \int_\Omega \omega^* b \, d\Omega + \int_\Gamma \left(\omega^* V w + w_{,n} M \omega^* - \omega^*_{,n} M w - w V \omega^* \right) ds - \sum_k \left(\omega^* [\![T w]\!] - w [\![T \omega^*]\!] \right)_k, \quad (3\text{-}4)$$

in which $w^* = w^*(\boldsymbol{x}, \boldsymbol{y})$, for $\boldsymbol{x}, \boldsymbol{y} \in \Gamma$, is the fundamental solution and ω^* its normal derivative at point $\boldsymbol{x} \in \Gamma$:

$$w^* = \frac{1}{8\pi} r^2 \ln r, \qquad \omega^* = \left(\frac{1}{8\pi} r^2 \ln r \right)_{,\boldsymbol{\nu}} = \frac{1}{8\pi} r r_{,\boldsymbol{\nu}} (2 \ln r + 1). \quad (3\text{-}5)$$

$\boldsymbol{\nu}$ being the unit normal vector to the boundary at point $\boldsymbol{x}$, whereas $\boldsymbol{n}$ is the unit normal vector to the boundary at the integration point $\boldsymbol{y}$, and $r = \|\boldsymbol{x} - \boldsymbol{y}\|$ (Figure 2, left).

Equations (3-3) and (3-4) can be used to establish the boundary quantities not specified. They are solved numerically using the BEM. The boundary integrals are approximated using N constant boundary elements, whereas the domain integrals are approximated using M linear triangular elements. The domain discretization is performed automatically using the Delaunay triangulation. Since the fictitious source is not defined on the boundary, the nodal points of the triangles adjacent to the boundary are placed on their sides (Figure 2, right).

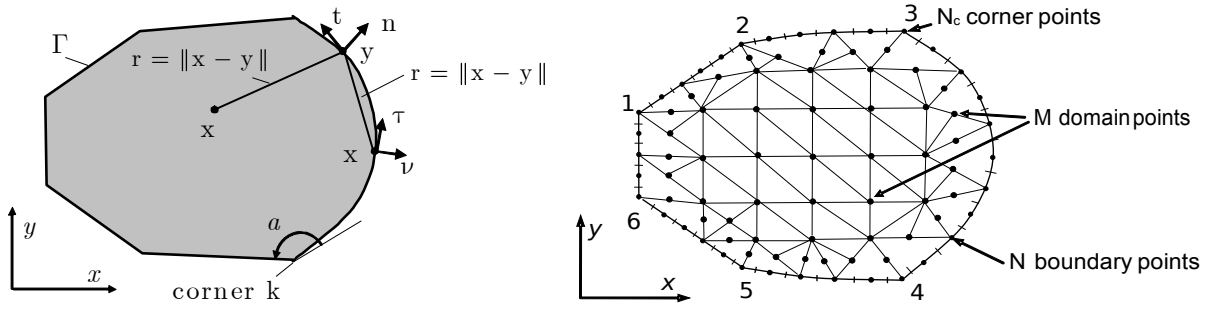

Figure 2. Left: BEM notation. Right: Boundary and domain discretization.

Thus, after discretization and application of the boundary integral equations (3-3) and (3-4) at the N boundary nodal points and (3-3) at the N_c corner points we obtain

$$\boldsymbol{H}\begin{Bmatrix}\boldsymbol{w}\\ \boldsymbol{w}_c\\ \boldsymbol{w}_{,n}\end{Bmatrix}=\boldsymbol{G}\begin{Bmatrix}\boldsymbol{V}\\ \boldsymbol{R}\\ \boldsymbol{M}\end{Bmatrix}+\boldsymbol{A}\boldsymbol{b}, \tag{3-6}$$

where $\boldsymbol{H}$, $\boldsymbol{G}$ are $N\times N$ known coefficient matrices originating from the integration of the kernel functions on the boundary elements, $\boldsymbol{A}$ is an $N\times M$ coefficient matrix originating from the integration of the kernel function on the domain elements, $\boldsymbol{w}$, $\boldsymbol{w}_c$, $\boldsymbol{w}_{,n}$ are the vectors of the N boundary nodal displacements, N_c corner displacements and N boundary nodal normal slopes, respectively, $\boldsymbol{V}$, $\boldsymbol{R}$, $\boldsymbol{M}$ are the vectors of the N nodal values of effective shear force, N_c concentrated corner forces, and N nodal values of the normal bending moment, and $\boldsymbol{b}$ is the vector of the M nodal values of the fictitious source.

Equation (3-6) constitutes a system of $2N+N_c$ equations for $4N+2N_c+M$ unknowns. Additional $2N+N_c$ equations are obtained from the boundary conditions. Thus, the boundary conditions (2-10), when applied at the N boundary nodal points and the N_c corner points yield the equations

$$\alpha_1\boldsymbol{w}+\alpha_2\boldsymbol{w}_{,n}+\alpha_3\boldsymbol{V}=\boldsymbol{0},\qquad \beta_1\boldsymbol{w}_{,n}+\beta_2\boldsymbol{M}=\boldsymbol{0},\qquad \boldsymbol{c}_1\boldsymbol{w}_c+\boldsymbol{c}_2\boldsymbol{R}=\boldsymbol{0}, \tag{3-7}$$

where α_1, α_2, α_3, β_1, β_2, $\boldsymbol{c}_1$, $\boldsymbol{c}_2$ are known coefficient matrices. Note that the first equation in (3-7) has resulted after approximating the derivative $w_{,t}$ in (2-10a) with a finite difference scheme.

Equations (3-6) and (3-7) can be combined and solved for the boundary quantities $\boldsymbol{w}$, $\boldsymbol{w}_c$, $\boldsymbol{w}_{,n}$, $\boldsymbol{V}$, $\boldsymbol{R}$, $\boldsymbol{M}$ in terms of the fictitious load $\boldsymbol{b}$. Subsequently, these expressions are used to eliminate the boundary quantities from the discretized counterpart of (3-2). Thus we obtain the following representation for the deflection

$$w(\boldsymbol{x},t)=\sum_{k=1}^{M}b_k(t)W_k(\boldsymbol{x}),\quad \boldsymbol{x}\in\Omega. \tag{3-8}$$

The derivatives of $w(\boldsymbol{x})$ at points $\boldsymbol{x}$ inside Ω are obtained by direct differentiation of (3-2). Thus, we obtain after elimination of the boundary quantities

$$w_{,pqr}(\boldsymbol{x},t)=\sum_{k=1}^{M}b_k(t)W_{k,pqr}(\boldsymbol{x}),\quad p,q,r\in\{0,x,y\},\ \boldsymbol{x}\in\Omega, \tag{3-9}$$

3.2. ***The plane stress problem.*** Noting that Equations (2-11) are of the second order their analog equations are obtained using the Laplace operator. This yields

$$\nabla^2u=b_1(\boldsymbol{x},t),\qquad \nabla^2v=b_2(\boldsymbol{x},t). \tag{3-10}$$

Setting $q=u_{,n}$, the integral representation of the solution of the first of these equations is

$$\varepsilon u(\boldsymbol{x},t)=\int_\Omega v^*b_1\,d\Omega-\int_\Gamma(v^*q-q^*u)\,ds\quad \boldsymbol{x}\in\Omega\cup\Gamma \tag{3-11}$$

in which $v^*=\ell nr/2\pi$ is the fundamental solution to $\nabla^2u=b_1(\boldsymbol{x},t)$ and $q^*=v^*_{,n}$ its derivative normal to the boundary, $r=\|\boldsymbol{y}-\boldsymbol{x}\|\boldsymbol{x}\in\Omega\cup\Gamma$ and $\boldsymbol{y}\in\Gamma$, ε is the free term coefficient ($\varepsilon=1$ if $\boldsymbol{x}\in\Omega$, $\varepsilon=\frac{1}{2}$ if $\boldsymbol{x}\in\Gamma$ and $\varepsilon=0$ if $\boldsymbol{x}\notin\Omega\cup\Gamma$).

Using the BEM with constant boundary elements and linear triangular domain elements and following the same procedure applied for the plate equation, we obtain the following representation for the in-plane displacement u and its derivatives:

$$u_{,pq}(\boldsymbol{x},t)=\sum_{k=1}^{M} b_k^{(1)}(t)U_{k,pq}^{(1)}(\boldsymbol{x})+\sum_{k=1}^{M} b_k^{(2)}(t)U_{k,pq}^{(2)}(\boldsymbol{x})+U_{0,pq}(\boldsymbol{x}),\quad p,q\in\{0,x,y\},\ \boldsymbol{x}\in\Omega. \tag{3-12}$$

Similarly, we obtain for the displacement v

$$v_{,pq}(\boldsymbol{x},t)=\sum_{k=1}^{M} b_k^{(1)}(t)V_{k,pq}^{(1)}(\boldsymbol{x})+\sum_{k=1}^{M} b_k^{(2)}(t)V_{k,pq}^{(2)}(\boldsymbol{x})+V_{0,pq}(\boldsymbol{x}),\quad p,q\in\{0,x,y\},\ \boldsymbol{x}\in\Omega. \tag{3-13}$$

where $U_k^{(1)}$, $U_k^{(2)}$, $V_k^{(1)}$, $V_k^{(2)}$, U_0, V_0 are known functions. Note that U_0, V_0 result from the nonhomogeneous boundary conditions.

3.3. ***The final step of the AEM.*** Equations (3-9), (3-12) and (3-13) give the displacements $w(x,t)$, $u(x,t)$, $v(x,t)$ and their derivatives provided that the three fictitious sources $\boldsymbol{b}(t)$, $\boldsymbol{b}^{(1)}(t)$, $\boldsymbol{b}^{(2)}(t)$ are first established. This is achieved by working as following.

Collocating the PDEs (2-8) and (2-11) at the M internal nodal points and substituting the expressions (3-9) for the transverse deflection and the values (3-12), (3-13) for the membrane displacements, we obtain the following system of $3M$ nonlinear equations for $b_k(t)$, $b_k^{(1)}(t)$, $b_k^{(2)}(t)$, $(k=1,\ldots,M)$

$$\boldsymbol{M}\ddot{\boldsymbol{b}}+\boldsymbol{C}\dot{\boldsymbol{b}}+\boldsymbol{H}(\boldsymbol{b},\boldsymbol{b}^{(1)},\boldsymbol{b}^{(2)})=\boldsymbol{0}, \tag{3-14a}$$

$$\boldsymbol{A}_1\boldsymbol{b}^{(1)}+\boldsymbol{B}_1\boldsymbol{b}^{(2)}+\boldsymbol{H}_1(\boldsymbol{b})=\boldsymbol{G}_1, \tag{3-14b}$$

$$\boldsymbol{A}_2\boldsymbol{b}^{(1)}+\boldsymbol{B}_2\boldsymbol{b}^{(2)}+\boldsymbol{H}_2(\boldsymbol{b})=\boldsymbol{G}_2, \tag{3-14c}$$

where $\boldsymbol{M},\boldsymbol{C}$ are $M\times M$ known generalized mass and damping matrices, $\boldsymbol{H}$ is a generalized stiffness vector depending nonlinearly on the $\boldsymbol{b},\boldsymbol{b}^{(1)},\boldsymbol{b}^{(2)}$ and originates from the nonlinear terms of (2-8), $\boldsymbol{H}_1(\boldsymbol{b})$, $\boldsymbol{H}_2(\boldsymbol{b})$ are generalized stiffness vectors depending nonlinearly on $\boldsymbol{b}$ and originate from the nonlinear terms of (2-11), $\boldsymbol{A}_1$, $\boldsymbol{A}_2$, $\boldsymbol{B}_1$, $\boldsymbol{B}_2$ are $M\times M$ known matrices and originate from the linear terms of (2-11), and $\boldsymbol{G}_1$, $\boldsymbol{G}_2$ are vectors containing the in-plane loads. The expressions of these quantities are given in the Appendix.

Equation (3-14a) represents the semidiscretized equation of motion of the plate. The associated initial conditions are obtained by substituting (3-8) into (2-9):

$$\boldsymbol{b}(0)=\boldsymbol{W}^{-1}\boldsymbol{g}_1,\qquad \dot{\boldsymbol{b}}(0)=\boldsymbol{W}^{-1}\boldsymbol{g}_2, \tag{3-15}$$

where $\boldsymbol{W}$ is $M\times M$ known matrix and $\boldsymbol{g}_1$, $\boldsymbol{g}_2$ are vectors originating from (2-9).

3.4. ***The solution of the nonlinear equations of motion.*** Equations (3-14b) and (3-14c) are quasistatic and linear with respect to $\boldsymbol{b}^{(1)}$ and $\boldsymbol{b}^{(2)}$. Thus solving for these vectors and substituting in (3-14a) yields the equation of motion

$$\boldsymbol{M}\ddot{\boldsymbol{b}}+\boldsymbol{C}\dot{\boldsymbol{b}}+\boldsymbol{S}(\boldsymbol{b})=\boldsymbol{0}. \tag{3-16}$$

A time step integration for nonlinear equations can be employed to solve (3-16) with the initial conditions (3-15). The use however, of all the degrees of freedom may be computationally costly and in some

cases be inefficient due to the large number of coefficients $b_k(t)$. To overcome this difficulty in this investigation, the number of degrees of freedom is reduced using the Ritz transformation

$$\boldsymbol{b} = \Psi \boldsymbol{z}, \tag{3-17}$$

where $z_i(t)$ $(i = 1, \ldots, L < M)$ are new time-dependent parameters and Ψ is the $M \times L$ transformation matrix. Using this transformation, (3-16) and (3-15) are transformed into the reduced nonlinear initial value problem

$$\tilde{\boldsymbol{M}}\ddot{\boldsymbol{z}} + \tilde{\boldsymbol{C}}\dot{\boldsymbol{z}} + \tilde{\boldsymbol{S}}(\boldsymbol{z}) = \boldsymbol{0}, \tag{3-18a}$$

$$\boldsymbol{z}(0) = (\Psi^T\Psi)^{-1}\Psi^T\boldsymbol{W}^{-1}\boldsymbol{g}_1, \qquad \dot{\boldsymbol{z}}(0) = (\Psi^T\Psi)^{-1}\Psi^T\boldsymbol{W}^{-1}\boldsymbol{g}_2, \tag{3-18b}$$

where $\tilde{\boldsymbol{M}} = \Psi^T\boldsymbol{M}\Psi$, $\tilde{\boldsymbol{C}} = \Psi^T\boldsymbol{C}\Psi$, and $\tilde{\boldsymbol{S}}(z) = \Psi^T\boldsymbol{S}(b)$.

In this investigation the eigenmodes of the linear flutter plate problem near the critical load in absence of damping are selected as Ritz vectors [Guo and Mei 2003]. Equation (3-18a) under any specified initial conditions, say $g_1(\boldsymbol{x}) \neq 0$, $g_2(\boldsymbol{x}) = 0$, is solved and the postcritical response of the plate is studied by increasing the conservative and nonconservative loads. It is convenient to take the first mode of the linear problem as $g_1(\boldsymbol{x})$. The new AEM time step integration method developed for multiterm fractional differential equations [Katsikadelis 2009] has been employed to solve (3-18), because the modified Newton–Raphson method was not successful in all cases.

For the linear problem the nonlinear terms $\boldsymbol{H}_1(\boldsymbol{b})$, $\boldsymbol{H}_2(\boldsymbol{b})$ vanish and Equations (3-14b), (3-14c) can be solved independently to obtain the fictitious sources $\boldsymbol{b}_1$, $\boldsymbol{b}_2$. Moreover, (3-14a) becomes linear:

$$\boldsymbol{M}\ddot{\boldsymbol{b}} + \boldsymbol{C}\dot{\boldsymbol{b}} + (\boldsymbol{K} + \boldsymbol{F})\boldsymbol{b} = \boldsymbol{0}, \tag{3-19}$$

where $\boldsymbol{K}$ and $\boldsymbol{F}$ are linear generalized stiffness matrices given as

$$K_{ik} = D\delta_{ik}, \tag{3-20}$$

$$F_{ik} = (q_x^i + n_x^i)W_{ik,x} + (q_y^i + n_y^i)W_{ik,y} - N_x^i W_{ik,xx} - 2N_{xy}^i W_{ik,xy} - N_y^i W_{ik,yy}, \tag{3-21}$$

where $i, k = 1, \ldots, M$ and δ_{ik} the Kronecker delta.

This problem is solved by assuming a time harmonic solution

$$b_k(t) = \beta_k e^{i\lambda t}, \tag{3-22}$$

where β_k are parameters which do not depend on time and λ is the frequency of the vibration.

Substituting (3-22) into (3-19) we obtain the quadratic eigenvalue problem

$$(-\lambda^2\boldsymbol{M} + \lambda i\boldsymbol{C} + \boldsymbol{K} + \boldsymbol{F})\beta = \boldsymbol{0}, \tag{3-23}$$

where β is the vector containing the elements β_k. By increasing the conservative and nonconservative loads the imaginary part of frequency λ becomes negative and the plate becomes unstable. The obtained eigenmodes from the eigenvalue problem (3-23) in absence of damping and near the critical value are employed as Ritz vectors in (3-17).

4. Examples

On the base of the previously described procedure a FORTRAN code has been written for solving the nonlinear flutter instability problem for plates. The efficiency and accuracy of the method is demonstrated by the following examples.

Example 1. We study the stability of the square plate of Figure 3. The plate is subjected to a follower uniform in-plane line load along the free edge. The boundary conditions are also shown in the figure. Two types of in-plane boundary conditions, designated as case (i) and case (ii), are considered along the edges $x = 0$ and $y = 0, 4$. Case (i), though not realistic, has been studied because there are results in the literature for comparison. It should be noted that in this case the distribution of the membrane forces is uniform ($N_x = P$, $N_y = N_{xy} = 0$). In case (ii) the distribution of the membrane forces is nonuniform and it results from the simultaneous solution of the nonlinear plane stress problem. This is an advantage of the presented solution method, since it permits the investigation of the influence of the in-plane boundary conditions on the nonlinear flutter instability. The parameters used are

$$E = 30\,\text{GPa}, \quad h = 0.1\,\text{m}, \quad \nu = 0.3, \quad \rho = 10^4\,\text{kg/m}^3.$$

The results were obtained with $N = 276$ boundary elements and $M = 133$ internal collocation points (Figure 4, left).

Figure 4, right, shows the first two eigenfrequencies of the linear plate problem without damping as the follower load increases. Flutter instability occurs when two real frequencies coalesce and become complex conjugate. The linear flutter loads are for case (i) $P_{cr} = 8917\,\text{kN}$ (8868 kN [Adali 1982]) and for case (ii) $P_{cr} = 10400\,\text{kN}$. The modes of the linear eigenproblem obtained at (i) $P = 8800\,\text{kN}$ and (ii) $P = 10000\,\text{kN}$ were employed as Ritz vectors. Figure 5 shows the dependence of the maximum deflection at point A of the undamped plate on the follower force using different number of the linear modes. The use of more than 10 modes does not change the results considerably. Figure 6 shows the amplitude of the oscillations when external and internal damping is considered. Figure 7, left, shows the

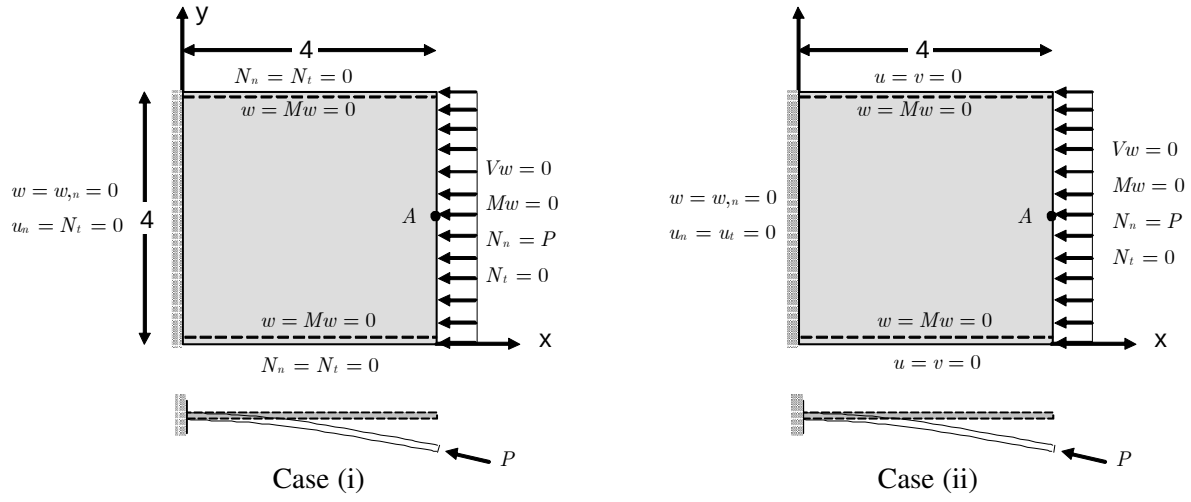

Figure 3. Geometry and boundary conditions of the plate in Example 1.

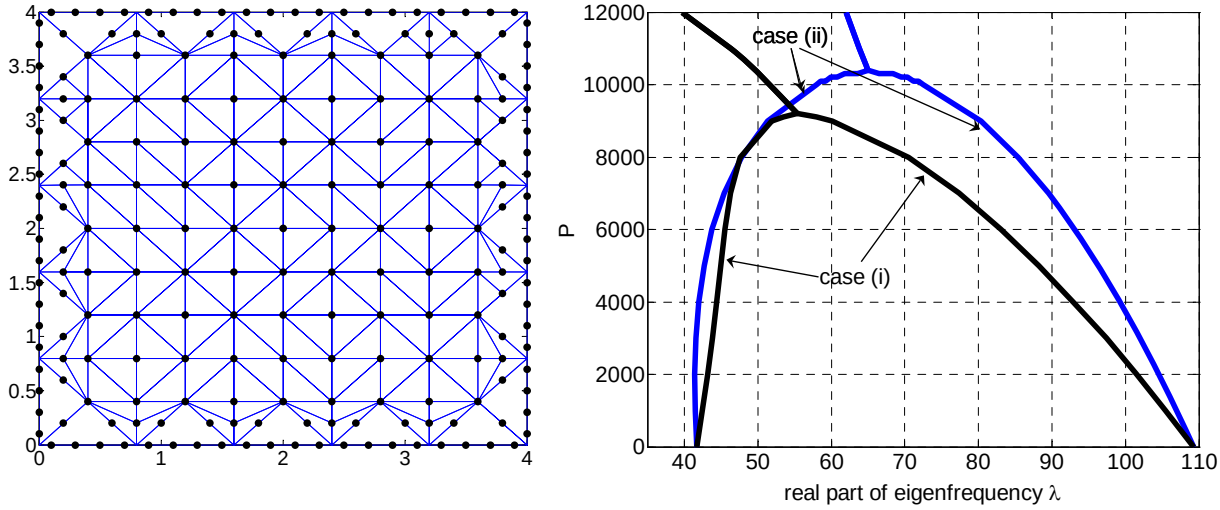

Figure 4. In reference to Example 1. Left: Boundary and domain nodal points. Right: Frequencies versus load.

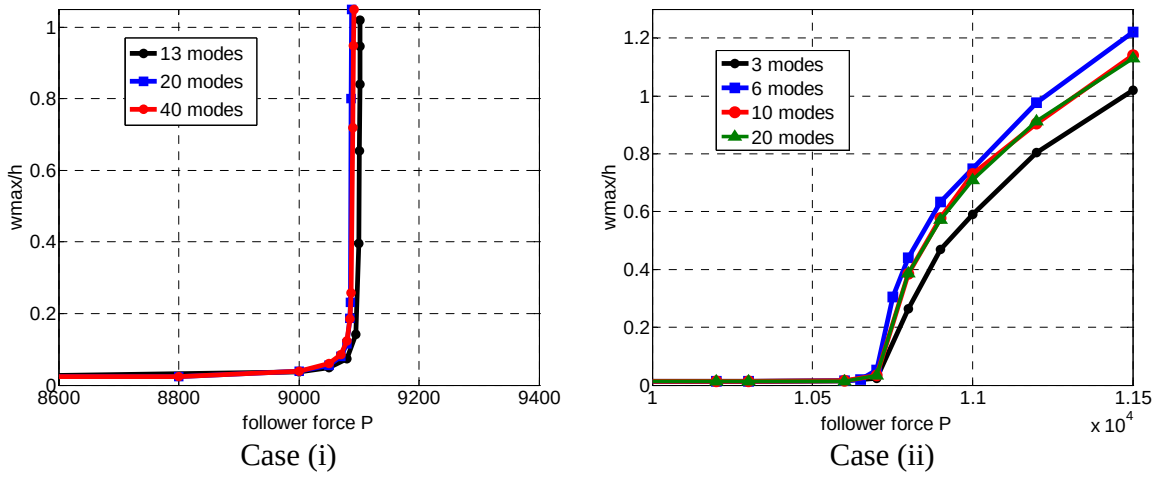

Figure 5. Maximum deflection at point A with different number of the linear modes employed for reduction of the degrees of freedom in the undamped plate in Example 1.

time history of the deflection at A on the free edge in case (ii) without ($c = 0$) and with external damping ($c = 2$). In the presence of damping (external or internal) the plate reaches a limit cycle oscillation. It is observed that viscous damping has a stabilizing effect while the structural damping destabilizes the plate. This result is in accordance with that reported by other researchers [Higuchi and Dowell 1992; Mei 1977]. Finally, Figure 7, right, shows the limit cycle of the deflection at point (3.2, 2); note that it is a Lamé curve with $n = 2.1$.

Example 2. The stability of the simply supported plate of Figure 8 is investigated. The plate is subjected to aerodynamic pressure due to steady supersonic air flow $q_x = 0.307\mu$, $q_y = 0$ and aerodynamic damping

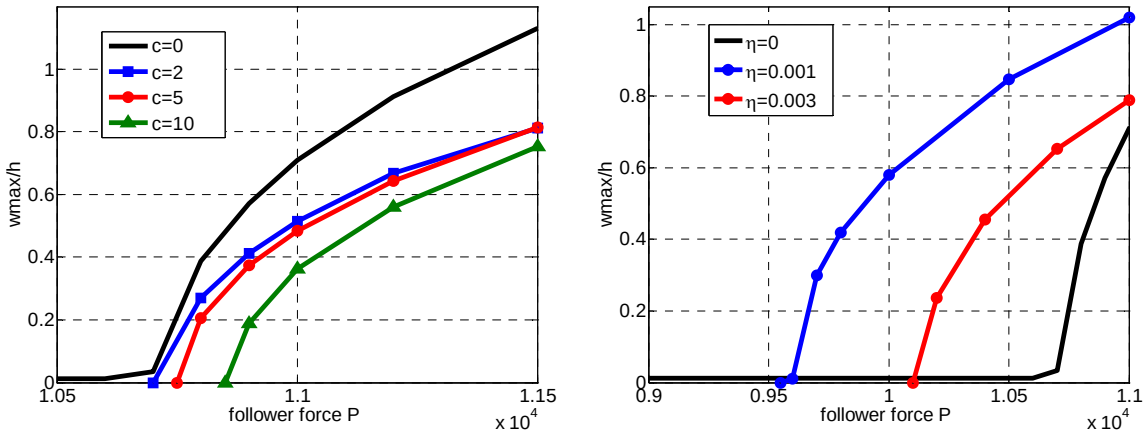

Figure 6. Amplitude of the limit cycle oscillation at point A for case (ii) (10 Ritz modes), with viscous damping (left) and with structural damping (right).

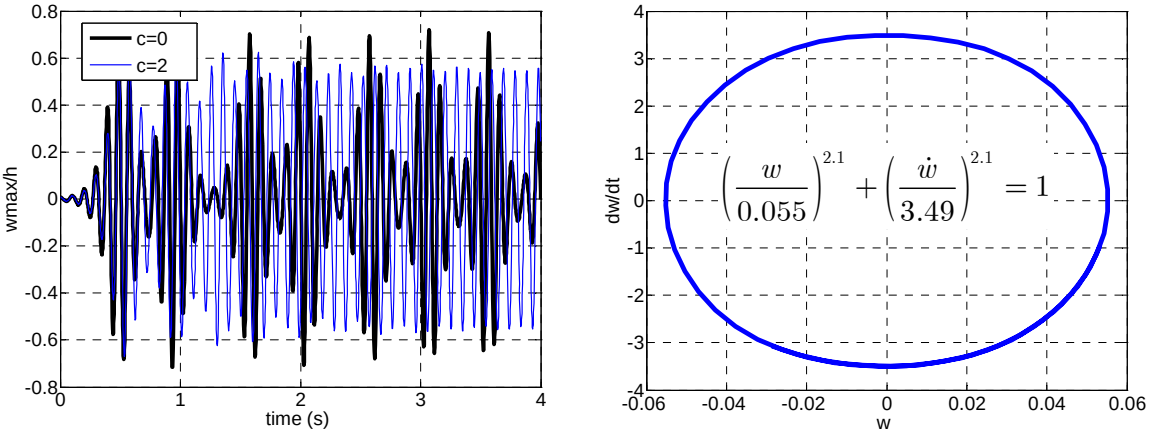

Figure 7. Left: Time history of the deflection at point (3.2, 2) with and without external damping. Right: Phase plane plot at point (3.2, 2) for external damping $c = 2$ for $t >$ 7 sec ($P = 11500$ kN/m, 10 Ritz modes, case (ii)).

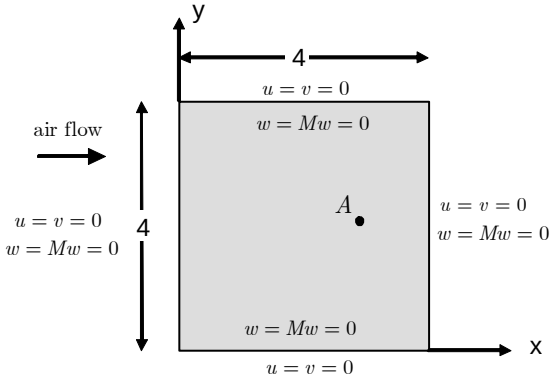

Figure 8. Simply supported immovable plate of Example 2.

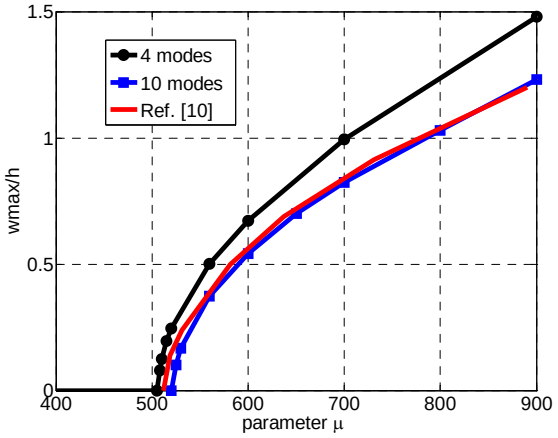

Figure 9. Amplitude of the limit cycles versus parameter μ at point $A(3, 2)$.

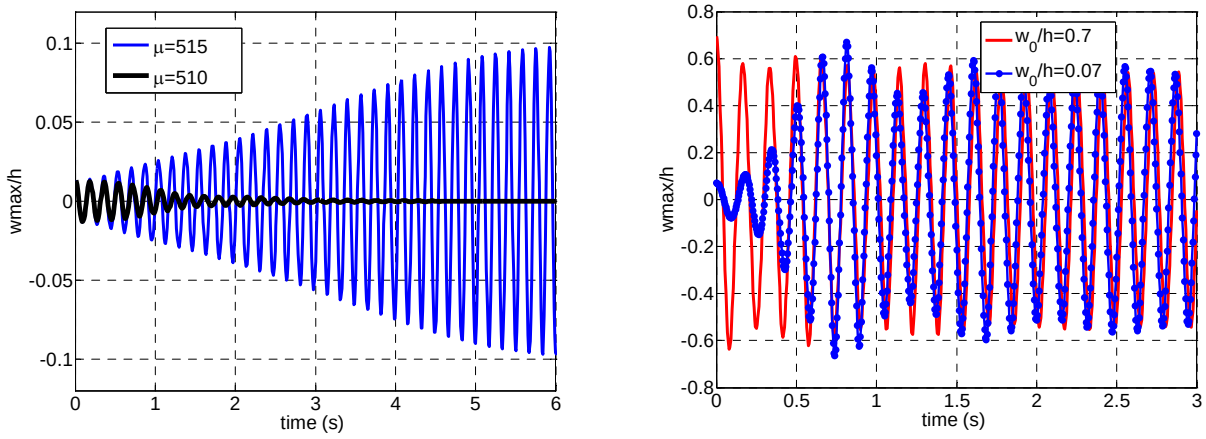

Figure 10. Left: Time history of the deflection at point A for two values of μ. Right: The effect of the initial conditions on limit cycle oscillations, for $\mu = 600$.

$c = 0.00857\sqrt{\mu}$, where μ is a nondimensional parameter which depends on the air flow velocity [Guo and Mei 2003]. The other parameters are

$$E = 210\,\text{GPa}, \quad h = 0.01\,\text{m}, \quad \nu = 0.33, \quad \rho = 10^4\,\text{kg/m}^3.$$

For the linear problem the critical value was found $\mu_{cr} = 519$ ($\mu_{cr} = 512$ in [Guo and Mei 2003]). Figure 9 shows the amplitude of the limit cycle oscillation at point $A(3, 2)$ with increasing parameter μ using 4 and 10 Ritz modes and a FEM solution [Guo and Mei 2003]. Figure 10 shows the time history of the deflection at point A for two values of μ, and then for two different initial conditions; from the graph on the right it is clear that the limit cycle oscillation is independent of the initial displacements. Figure 11 depicts the time history of the bending moment m_x and the membrane force N_x at point A for $\mu = 890$. Finally, in Figure 12 we see the phase plane plot at point A for $\mu = 890$, and the limit cycle, which is again a Lamé curve with $n = 2.8$.

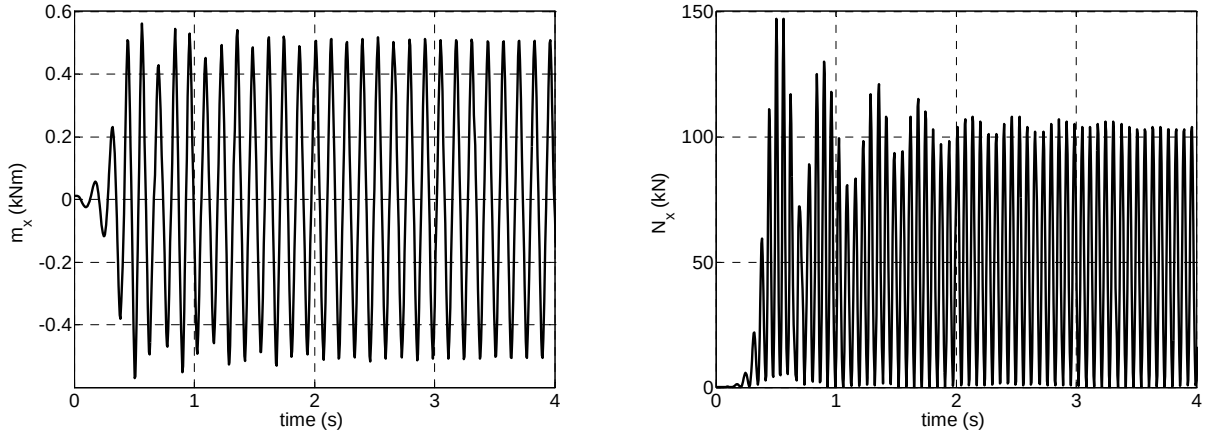

Figure 11. Time history of the bending moment m_x (left) and of the membrane force N_x (right) at point A, for $\mu = 890$.

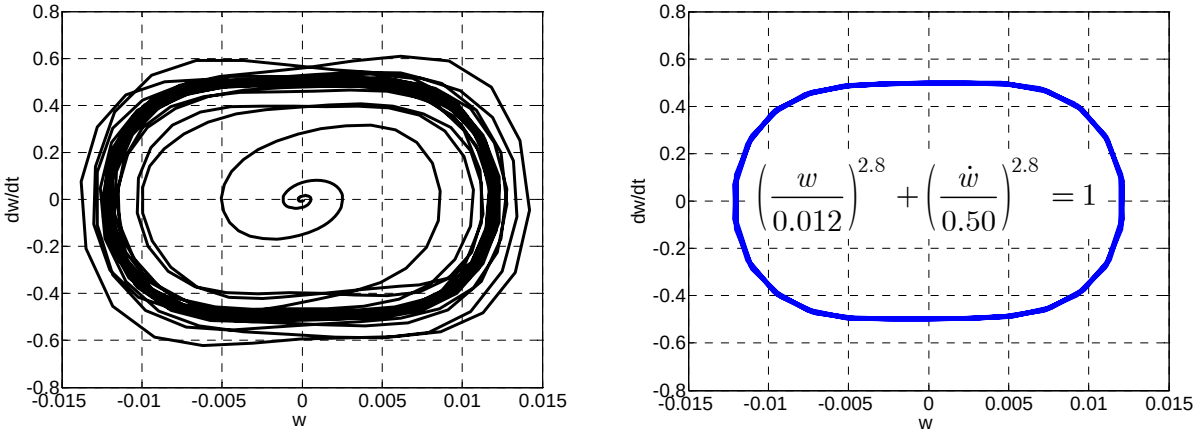

Figure 12. Phase plane plot at point A for $\mu = 890$ (10 modes) for $0 < t < 5$ (left) and $t > 4$ (right).

Example 3. The rectangular plate of Figure 13 is subjected to the combined action of aerodynamic pressure due to steady supersonic air flow $q_x = \mu$, $q_y = 0$ and a conservative in-plane line load along two opposite edges. The aerodynamic damping is $c = 0.1$. The other parameters used are

$$E = 210\,\text{GPa}, \quad h = 0.01\,\text{m}, \quad \nu = 0.3, \quad \rho = 7550\,\text{kg/m}^3.$$

The results were obtained with $N = 300$ boundary elements and $M = 253$ internal collocation points and 20 eigenmodes as Ritz vectors for reduction of the degrees of freedom. Figure 14 presents the stability regions with increasing aerodynamic pressure (nonconservative) and in-plane load (conservative). Figure 15 presents the time history of the deflection at the center of the plate in the case of divergence type of instability. In this case the plate buckles but remains in dynamic stable situation. Figure 16 shows the time history of the deflection of point $A(1.5, 2)$ in the case of flutter instability.

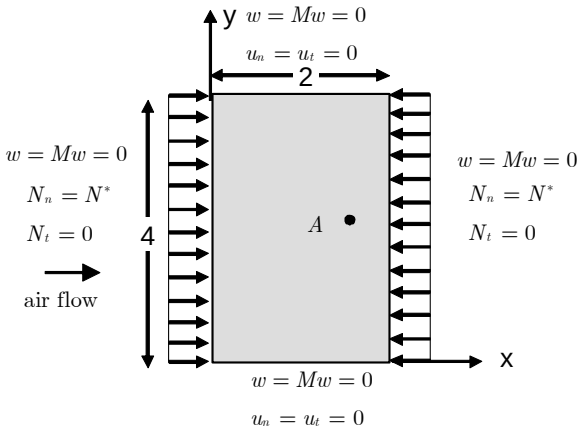

Figure 13. Geometry and boundary conditions of the plate in Example 3.

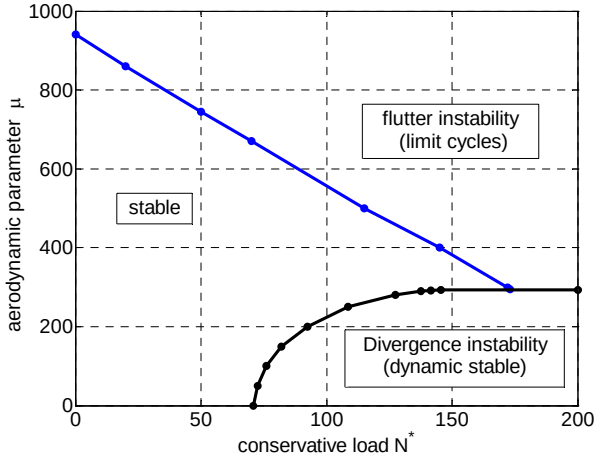

Figure 14. Stability regions for the combined action of nonconservative (aerodynamic pressure) and conservative loads.

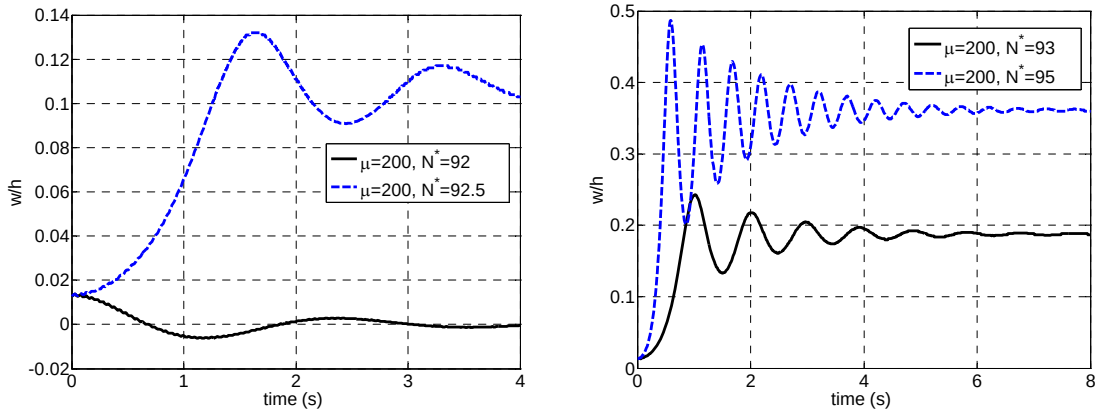

Figure 15. Time history of the deflection at the center of the plate ($\mu = 200$) for $N^* = 92, 92.5$ (left) and $N^* = 93, 95$ (right).

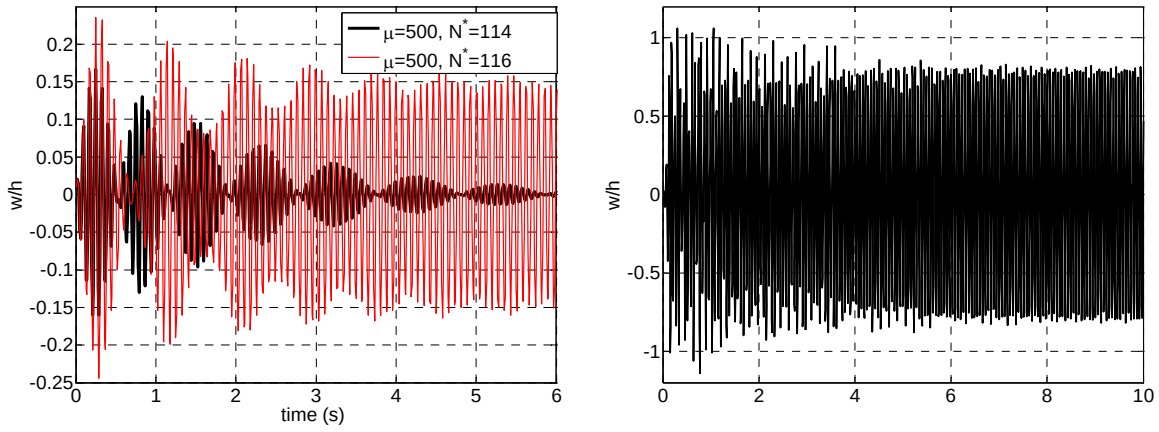

Figure 16. Time history of the deflection at point A for $\mu = 500$, $N^* = 114, 116$ (left) and $\mu = 700$, $N^* = 100$ (right).

Example 4. The cantilever plate of Figure 17, left, is subjected to aerodynamic pressure due to steady supersonic air flow $q_x = 0$, $q_y = 0.031v^2$, where v is the air velocity. The other parameters used are $E = 210\,\text{GPa}$, $h = 0.01\,\text{m}$, $\nu = 0.3$, $\rho = 7550\,\text{kg/m}^3$. The results were obtained with $N = 385$ boundary elements and $M = 125$ internal collocation points and 20 eigenmodes as Ritz vectors for reduction of the degrees of freedom. Figure 18 on the preceding page presents the frequencies of the linear plate

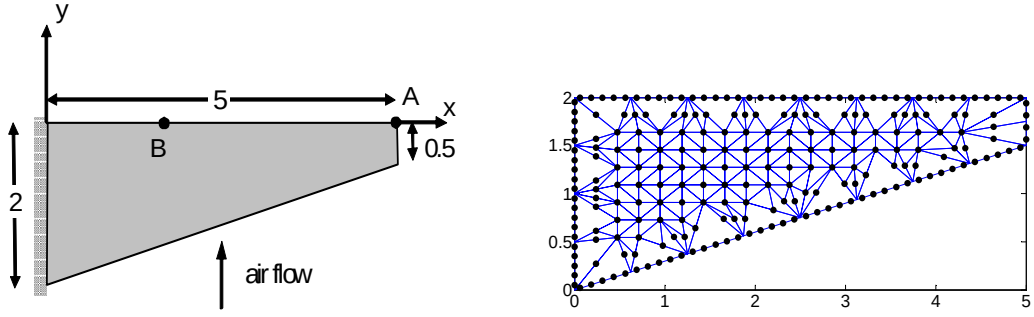

Figure 17. Left: Cantilever plate of Example 4. Right: Boundary and domain nodal points.

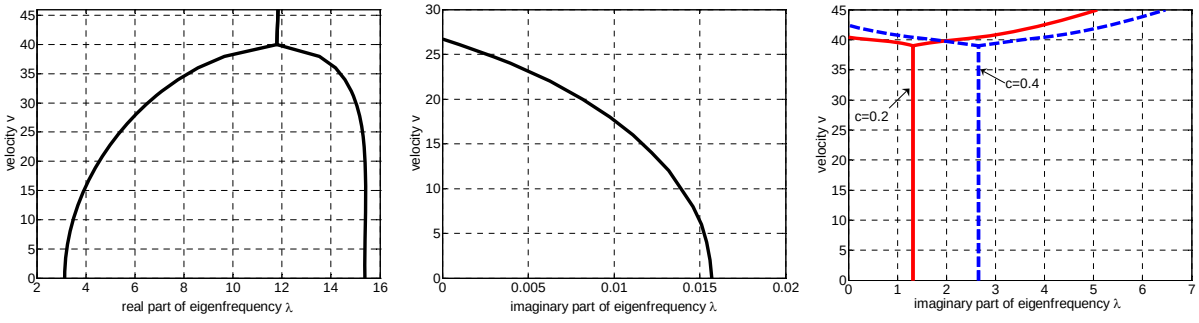

Figure 18. Frequency vs. air velocity for the linear plate problem with no damping (left), structural damping $\eta = 0.01$ (middle), and viscous damping $c = 0.2$, 0.4 (right).

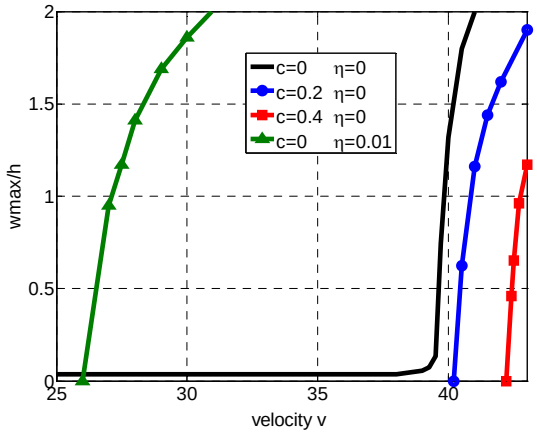

Figure 19. Maximum deflection in absence of damping and amplitude of the limit cycles in presence of damping versus air velocity v at corner point A.

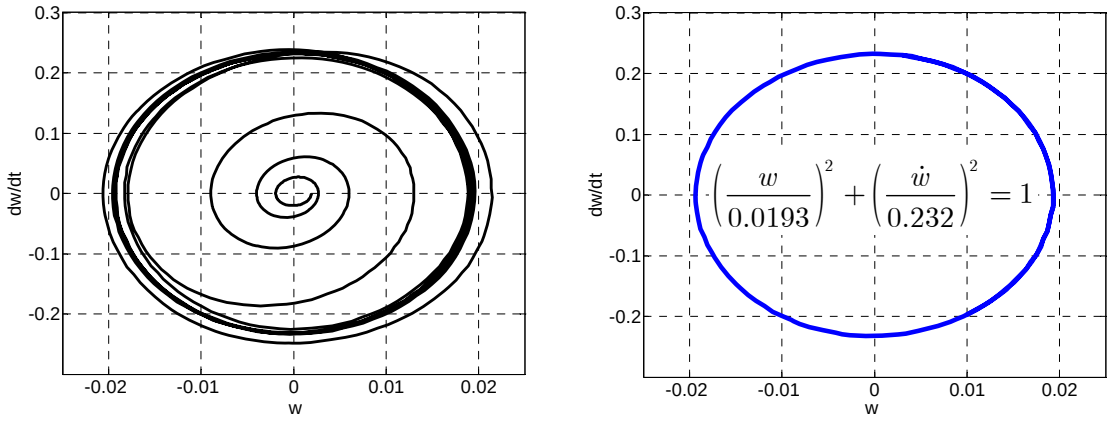

Figure 20. Phase plane plot at point (5, 2) with external damping $c = 0.2$ for $0 < t < 8$ sec (left) and $t > 7$ sec (right), with $v = 43$ m/s and 20 Ritz modes.

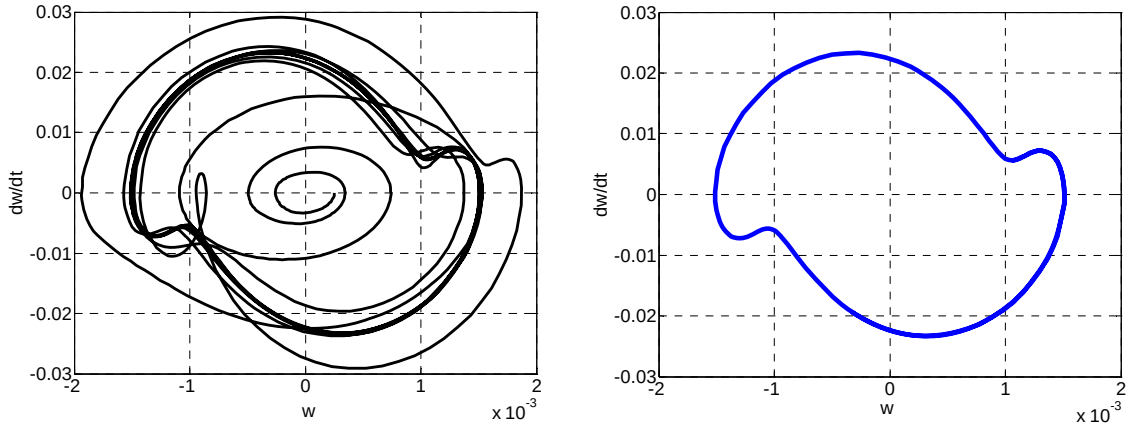

Figure 21. Phase plane plot at point (2, 2) with external damping $c = 0.2$ for $0 < t < 8$ sec (left) and $t > 7$ sec (right), with $v = 43$ m/s and 20 Ritz modes.

problem as the air velocity increases in absence of damping and for various values of external (viscous) and internal (structural) damping. The linear flutter velocity is $v_{cr} = 38.9$ m/s in absence of damping, $v_{cr} = 40.5$ m/s with external damping $c = 0.2$, $v_{cr} = 42.3$ m/s with external damping $c = 0.4$ and $v_{cr} = 26.7$ m/s with internal damping $\eta = 0.01$. Figure 19 presents the maximum deflection at point A in absence of damping and the amplitude of the limit cycles in presence of internal or external damping for various values of the flow velocity. Figures 20 and 21 show the phase plot at points A and B respectively when $v = 43$ m/s and $c = 0.2$. At point A the limit cycle is a Lamé curve with $n = 2$ (ellipse).

5. Conclusions

Nonlinear flutter instability of thin plates of arbitrary geometry subjected to general types of boundary conditions, under both interior as well as edge conservative and nonconservative loads, and in the presence of external and internal damping, has been investigated in this work. Solution of this problem is achieved by the AEM, an integral equation method that converts coupled nonlinear PDEs describing the response of the plate into uncoupled, linear PDEs that are subsequently treated by the D/BEM. More specifically, the semidiscretized nonlinear equations of motion give rise to an initial-value problem that is efficiently solved using a small set of modes near the critical point as Ritz vectors in conjunction with a novel time stepping algorithm.

As far as numerical implementation was concerned, the influence of in-plane boundary conditions that appears in realistic formulations of plate aeroelasticity problems on flutter instability was investigated. Certain findings on the nonlinear flutter instability reported earlier by other researchers that were based on simple engineering models were validated. Among them is the stabilizing effect of external (viscous) damping in contrast to the destabilizing effect of internal (structural) damping. Also, the combined action of conservative and nonconservative loads was studied, which may lead to divergence or flutter instability in the plate. In closing, the methodology presented herein yields an efficient computational tool for studying complex problems stemming from the nonlinear dynamic response of thin plates subjected to conservative and nonconservative loads.

Appendix: Expressions for the matrices (3-14)

The indices i and k range from 1 to M.

$$M_{ik} = \rho_i h W_{ik}, \qquad C_{ik} = c_i W_{ik},$$

$$H^i = -N_x^i \sum_{k=1}^{M} W_{ik,xx} b_k - 2N_{xy}^i \sum_{k=1}^{M} W_{ik,xy} b_k - N_y^i \sum_{k=1}^{M} W_{ik,yy} b_k + (q_x^i + n_x^i) \sum_{k=1}^{M} W_{ik,x} b_k + (q_y^i + n_y^i) \sum_{k=1}^{M} W_{ik,y} b_k,$$

$$A_{1ik} = \delta_{ik} + \frac{1+\nu}{1-\nu}\left(U_{ik,xx}^{(1)} + V_{ik,xy}^{(1)}\right), \qquad B_{1ik} = \frac{1+\nu}{1-\nu}\left(U_{ik,xx}^{(2)} + V_{ik,xy}^{(2)}\right),$$

$$A_{2ik} = \frac{1+\nu}{1-\nu}\left(U_{ik,xy}^{(1)} + V_{ik,yy}^{(1)}\right), \qquad B_{2ik} = \delta_{ik} + \frac{1+\nu}{1-\nu}\left(U_{ik,xy}^{(2)} + V_{ik,yy}^{(2)}\right),$$

$$G_1^i = -\frac{n_x^i + p_x^i}{Gh} - \frac{1+\nu}{1-\nu}(U_{0i,xx} + V_{0i,xy}), \qquad G_2^i = -\frac{n_y^i + p_y^i}{Gh} - \frac{1+\nu}{1-\nu}(U_{0i,xy} + V_{0i,yy}),$$

$$H_1^i = \left(\frac{2}{1-\nu}\sum_{k=1}^{M} W_{ik,xx}b_k + \sum_{k=1}^{M} W_{ik,yy}b_k\right)\sum_{k=1}^{M} W_{ik,x}b_k + \frac{1+\nu}{1-\nu}\sum_{k=1}^{M} W_{ik,xy}b_k \sum_{k=1}^{M} W_{ik,y}b_k,$$

$$H_2^i = \left(\frac{2}{1-\nu}\sum_{k=1}^{M} W_{ik,yy}b_k + \sum_{k=1}^{M} W_{ik,xx}b_k\right)\sum_{k=1}^{M} W_{ik,y}b_k + \frac{1+\nu}{1-\nu}\sum_{k=1}^{M} W_{ik,xy}b_k \sum_{k=1}^{M} W_{ik,x}b_k,$$

where

$$N_x^i = C\left(\sum_{k=1}^{M}(U_{ik,x}^{(1)} + \nu V_{ik,y}^{(1)})b_k^{(1)} + \sum_{k=1}^{M}(U_{ik,x}^{(2)} + \nu V_{ik,y}^{(2)})b_k^{(2)} + U_{0i,x} + \nu V_{0i,y} + \tfrac{1}{2}\Big(\sum_{k=1}^{M} W_{ik,x}b_k\Big)^2 + \tfrac{1}{2}\nu\Big(\sum_{k=1}^{M} W_{ik,y}b_k\Big)^2\right),$$

$$N_y^i = C\left(\sum_{k=1}^{M}(\nu U_{ik,x}^{(1)} + V_{ik,y}^{(1)})b_k^{(1)} + \sum_{k=1}^{M}(\nu U_{ik,x}^{(2)} + V_{ik,y}^{(2)})b_k^{(2)} + \nu U_{0i,x} + V_{0i,y} + \tfrac{1}{2}\nu\Big(\sum_{k=1}^{M} W_{ik,x}b_k\Big)^2 + \tfrac{1}{2}\Big(\sum_{k=1}^{M} W_{ik,y}b_k\Big)^2\right),$$

$$N_{xy}^i = C\frac{1-\nu}{2}\left(\sum_{k=1}^{M}(U_{ik,y}^{(1)} + V_{ik,x}^{(1)})b_k^{(1)} + \sum_{k=1}^{M}(U_{ik,y}^{(2)} + V_{ik,x}^{(2)})b_k^{(2)} + U_{0i,y} + V_{0i,x} + \sum_{k=1}^{M} W_{ik,x}b_k \sum_{k=1}^{M} W_{ik,y}b_k\right).$$

References

[Adali 1982] S. Adali, "Stability of a rectangular plate under nonconservative and conservative forces", *Int. J. Solids Struct.* **18**:12 (1982), 1043–1052.

[Babouskos and Katsikadelis 2009] N. Babouskos and J. T. Katsikadelis, "Flutter instability of damped plates under combined conservative and nonconservative loads", *Arch. Appl. Mech.* **79**:6–7 (2009), 541–556.

[Chen et al. 2008] D. Chen, Y. Yang, and C. Fan, "Nonlinear flutter of a two-dimension thin plate subjected to aerodynamic heating by differential quadrature method", *Acta Mech. Sinica* **24**:1 (2008), 45–50.

[Dowell 1966] E. H. Dowell, "Nonlinear oscillations of a fluttering plate", *AIAA J.* **4**:7 (1966), 1267–1275.

[Guo and Mei 2003] X. Guo and C. Mei, "Using aeroelastic modes for nonlinear panel flutter at arbitrary supersonic yawed angle", *AIAA J.* **41**:2 (2003), 272–279.

[Higuchi and Dowell 1992] K. Higuchi and E. H. Dowell, "Effect of structural damping on flutter of plates with a follower force", *AIAA J.* **30**:3 (1992), 820–825.

[Katsikadelis 1994] J. T. Katsikadelis, "The analog equation method: a powerful BEM-based solution technique for solving linear and nonlinear engineering problems", pp. 167–182 in *Boundary element method XVI* (Southampton, 1994), edited by C. A. Brebbia, Computational Mechanics Publications, Southampton, 1994.

[Katsikadelis 2002] J. T. Katsikadelis, "The analog boundary integral equation method for nonlinear static and dynamic problems in continuum mechanics", *J. Theor. Appl. Mech.* (*Warsaw*) **40** (2002), 961–984.

[Katsikadelis 2009] J. T. Katsikadelis, "Numerical solution of multi-term fractional differential equations", *Z. Angew. Math. Mech.* **89**:7 (2009), 593–608.

[Kim and Kim 2000] J. H. Kim and H. S. Kim, "A study on the dynamic stability of plates under a follower force", *Comput. Struct.* **74**:3 (2000), 351–363.

[Leipholz and Pfendt 1983] H. Leipholz and F. Pfendt, "Application of extended equations of Galerkin to stability problems of rectangular plates with free edges and subjected to uniformly distributed follower forces", *Comput. Methods Appl. Mech. Eng.* **37**:3 (1983), 341–365.

[Mei 1977] C. Mei, "A finite-element approach for nonlinear panel flutter", *AIAA J.* **15**:8 (1977), 1107–1110.

[Shiau and Lu 1990] L. C. Shiau and L. T. Lu, "Nonlinear flutter of composite laminated plates", *Math. Comput. Model.* **14** (1990), 983–988.

[Weiliang and Dowell 1991] Y. Weiliang and E. Dowell, "Limit cycle oscillation of a fluttering cantilever plate", *AIAA J.* **29**:11 (1991), 1929–1936.

[Zuo and Schreyer 1996] Q. H. Zuo and H. L. Schreyer, "Flutter and divergence instability of nonconservative beams and plates", *Int. J. Solids Struct.* **33**:9 (1996), 1355–1367.

Received 10 Oct 2008. Revised 7 Mar 2009. Accepted 9 Mar 2009.

JOHN T. KATSIKADELIS: jkats@central.ntua.gr
Academy of Athens, Office of Theoretical and Applied Mechanics, 4 Soranou Efesiou,, 11527 Athens, Greece

and

National Technical University of Athens, School of Civil Engineering, Heroon Polytechniou 9, 15780 Athens, Greece

NICK G. BABOUSKOS: babouskosn@yahoo.gr
National Technical University of Athens, School of Civil Engineering, Heroon Polytechniou 9, 15773 Athens, Greece